Received: 4 March 2021 | Revised: 15 April 2021 | Accepted: 23 April 2021

DOI: 10.1002/jbm.a.37212

ORIGINAL ARTICLE

Biomimetic sponges improve muscle structure and function following volumetric muscle loss

Gabriel Haas[1] | Andrew Dunn[1] | Josh Madsen[1] | Peter Genovese[1] | Hannah Chauvin[1] | Jeffrey Au[1] | Natalia Ziemkiewicz[1] | David Johnson[1] | Allison Paoli[1] | Andrew Lin[1] | Nicholas Pullen[2] | Koyal Garg[1]

[1]Department of Biomedical Engineering, Parks College of Engineering, Aviation, and Technology, Saint Louis University, St. Louis, Missouri

[2]School of Biological Sciences, College of Natural and Health Sciences, University of Northern Colorado, Greeley, Colorado

Correspondence
Koyal Garg, PhD, Assistant Professor, Department of Biomedical Engineering, Parks College of Engineering, Aviation, and Technology, 3507 Lindell Blvd, St. Louis, MO 63103, USA.
Email: koyal.garg@slu.edu

Funding information
National Institutes of General Medical Sciences (NIH), Grant/Award Number: 1R15GM129731

Abstract

Skeletal muscle is inept in regenerating after traumatic injuries such as volumetric muscle loss (VML) due to significant loss of various cellular and acellular components. Currently, there are no approved therapies for the treatment of muscle tissue following trauma. In this study, biomimetic sponges composed of gelatin, collagen, laminin-111, and FK-506 were used for the treatment of VML in a rodent model. We observed that biomimetic sponge treatment improved muscle structure and function while modulating inflammation and limiting the extent of fibrotic tissue deposition. Specifically, sponge treatment increased the total number of myofibers, type 2B fiber cross-sectional area, myosin: collagen ratio, myofibers with central nuclei, and peak isometric torque compared to untreated VML injured muscles. As an acellular scaffold, biomimetic sponges may provide a promising clinical therapy for VML.

KEYWORDS
extracellular matrix, inflammation, volumetric muscle loss

1 | INTRODUCTION

Skeletal muscle is endowed with a remarkable capacity for regeneration, but "volumetric muscle loss" (VML) presents a unique challenge due to the significant loss of various cellular and acellular components such as basal lamina, resident stem cell (or satellite cell) population, neuromuscular junctions, and vasculature. As a result, VML results in chronic functional impairment and disability.[1-4] Autologous tissue grafts from an uninjured site are currently used to treat VML injuries in the clinic.[5] However, this complicated surgical approach can cause donor site morbidity, infection, and has been reported to result in graft failure in 4–7% of cases.[6,7] Physical therapy is typically recommended to VML patients to strengthen the remaining muscle mass, but it is unable to facilitate appreciable muscle regeneration within the site of injury.[8] Therefore, there is a clinical need to develop bioengineered therapies for muscle regeneration and reconstruction following VML.

The extracellular matrix (ECM) forms an ideal microenvironment for cell survival and activity. The ECM not only provides a framework for structural and mechanical support but also cellular attachment, signaling, and activity.[9,10] As a result, acellular ECM scaffolds have been extensively used for the treatment of skeletal muscle injuries. However, there is mounting evidence to suggest that decellularized ECM scaffolds do not support robust muscle regeneration and often remodel into a dense collagenous scar.[11-14]

In a previous study, we developed biomimetic sponges composed of gelatin, collagen, and laminin-111 cross-linked together with 1-ethyl-3-[3-dimethyl aminopropyl] carbodiimide (EDC). The ECM proteins were chosen based on their abundance in the native skeletal muscle structure[15-18] and documented success in promoting muscle repair in previous studies. For instance, gelatin is a denatured form of collagen that retains its biocompatibility and offers a less expensive alternative to collagen.[19] Gelatin sponges have been used in a variety

Gabriel Haas and Andrew Dunn contributed equally to this study.

of tissue engineering applications.[19-23] Gelfoam® is a gelatin sponge prepared from type A porcine gelatin that has widely been used in the clinic to control bleeding as a wound dressing.[24] Gelatin based scaffolds have been successfully used in combination with growth factors such as insulin-like growth factor[25] or fibroblast growth factor 2 (FGF-2)[26] for muscle tissue engineering. Collagen is widely used in the form of gels,[27] electrospun scaffolds,[28] and sponges[29] for skeletal muscle tissue engineering applications. In a rabbit model, a freeze-dried collagen sponge implanted into a partial-thickness VML defect showed less scar tissue formation and a greater number of regenerating myofibers compared to the unrepaired control at 24 weeks post-injury.[30] Laminin (LM)-111 is an embryonic isoform of laminin that is absent in adult tissues. LM-111 supplementation has demonstrated remarkable regenerative capacity in several models of disease[16,17,31] and injury,[32] primarily by upregulating α7 integrin protein expression in the myofiber and influencing satellite cell activity.

Biomimetic sponges offer several advantages over decellularized ECM scaffolds. Biomimetic sponges are fabricated via lyophilization (or freeze-drying) of polymer network, which yields a sponge-like material with a highly porous microstructure. Biomimetic sponges have superior mechanical properties as they are cross-linked using EDC. Another advantage of biomimetic sponges includes consistent and scalable manufacturing in large quantities. Further optimization of this technology is also possible through incorporation and local delivery of cells, growth factors, and drugs. In a murine model of VML, biomimetic sponge implantation supported the infiltration of satellite cells, promoted myogenic protein expression, and myofiber regeneration in a mouse model of VML involving 10% muscle loss in the gastrocnemius-soleus complex[33] on day 14 post-injury. However, only one early time-point was chosen for analysis and muscle function was not assessed.

In this study, we determine the extent to which biomimetic sponges will support muscle regeneration and function in a larger and more challenging animal model of VML involving 20% muscle loss in the rat tibialis anterior (TA) muscle. We also incorporated FK-506 in the biomimetic sponges to enhance their immunomodulatory properties during the acute phase (~7 days) post-VML injury. The fungal macrolide FK-506 (Tacrolimus) is an FDA approved immunosuppressant[34] that can modulate both innate and adaptive immune cell function.[35,36,37] In a previous study, systemic administration of FK-506 (1 mg/kg) in VML injured rats reduced the local immune response but did not improve muscle regeneration or function.[37] We hypothesize that FK-506 loaded biomimetic sponges will support functional recovery in a rat model of VML by stimulating regeneration and limiting the extent of inflammation and fibrosis.

2 | METHODS

2.1 | Preparation of biomimetic sponges with FK-506

A 3 wt% porcine skin gelatin (Sigma–Aldrich) solution was prepared in deionized (DI) water and heated to 60°C. After the gelatin had completely dissolved, the solution was allowed to cool to 50°C. The cooled gelatin solution was combined with 20 mM of EDC. Rat tail collagen I (Gibco, 3 mg/ml) was mixed with the gelatin solution at a ratio of 70:30 by volume. LM-111 (Trevigen) were added to the solution at final concentrations of 50 μg/ml. FK-506 (Abcam) was added at a final concentration of 25 μM, respectively. The solution was then aliquoted into a 48-well plate at 700 μl/well. The well plate was placed in a 100% methanol bath, allowing the sponges to gel at 4°C for 30 min, followed by overnight freezing at −8°C. The well plate was then removed from the bath and moved to a − 80°C freezer for 48 hr and subsequently lyophilized for at least 12 hr. Prior to in vitro culture or surgical implantation, the sponges were disinfected using ethanol and rinsed twice in sterile 1× phosphate-buffered saline (PBS).

2.2 | Measurement of FK-506 release

Biomimetic sponges loaded with FK-506 (0, 25, 50, and 100 μM) were fabricated in a 48 well-plate as described above. Following disinfection, the sponges were incubated in 500 μl of DMEM-F12 culture media (Gibco) at 37°C for 7 days ($n = 4$ per group/time-point). The media was collected, stored at −20°C, and replaced every day for 7 days. The media solution was diluted 1:25 and an ELISA kit (KA147, Abnova) was used for the quantification of FK-506 eluted from the sponges, as per manufacturer's instructions. The amount of FK-506 incorporated into each 700 μl sponge was calculated. The percentage of released FK-506 was determined by dividing the eluted and incorporated FK-506.

2.3 | Implantation of sponges into a VML model

This work was conducted in compliance with the Animal Welfare Act, the implementing Animal Welfare Regulations, and in accordance with the principles of the Guide for the Care and Use of Laboratory Animals. All animal procedures were approved by the Saint Louis University's Institutional Animal Care and Use Committee (animal protocol number 2645).

Male Lewis rats (10–12 weeks old) were purchased from Charles Laboratory and housed in a vivarium accredited by the Association for Assessment and Accreditation of Laboratory Animal Care International and provided with food and water ad libitum. Animals were randomly assigned to three experimental groups; age-matched cage controls, untreated VML, and sponge-treated VML. The animals were weighed prior to surgery and anesthetized using 2.5% isoflurane. The surgical site was aseptically prepared and a lateral incision was made through the skin to reveal the TA muscle, and the skin was separated from the musculature by blunt dissection. To create VML injury, a metal plate was inserted underneath the TA muscle, and a 6 mm punch biopsy was performed to remove approximately ~20% of the muscle mass. The biopsy was removed and weighed for consistency. A subset of injured animals received FK-506 (25 μM) loaded biomimetic sponges (6 mm disk)

while the other subset was left untreated ($n = 5–9$ animals per group). Bleeding was controlled with light pressure, and the skin incision was closed with simple interrupted skin staples. The animals were allowed to recover for 7, 14, or 28 days and euthanized via exsanguination followed by cervical dislocation.

The surgery was performed bilaterally, keeping the treatment subsets consistent between both legs. TA muscles were weighed upon collection ($n = 9–17$ muscles per group). From both VML injured hindlimbs, the top half of the TA muscle was preserved for histological analysis, and the bottom half was snap-frozen for biochemical analysis. This method of bilateral injury is also a desired means for the ethical reduction of study animal numbers, as published elsewhere.[38] The animals were identified by numbers and investigators were blinded to group allocation during data collection. At the time of surgery, the animals received sustained release buprenorphine (1 mg/kg) for pain control which was injected in the nape of the neck.

2.4 | Histology

TA muscles were cut in half at the defect site, and the upper portion was frozen in 2-methylbutane (Fisher Scientific) super-cooled in liquid nitrogen for 10 s. The muscles were mounted on stubs using OCT and transverse cross-sections (15 μm) were cryosectioned. Cross-sections were stained with hematoxylin and eosin (H&E), collagen 1 (1:100; ab34710; Abcam, Cambridge MA), sarcomeric myosin (1:50; MF20; Developmental Studies Hybridoma Bank), laminin (1:100; ab11575; Abcam; Cambridge MA), CD68 (1:50; MCA341R; AbD Serotec, Raleigh, NC), nuclei (DAPI; 1:100; Invitrogen), CD3 (1:100; ab5690; Abcam, Cambridge MA), CD31 (1:100; AF3628, R&D systems), α-bungarotoxin (1:100; B13422, Invitrogen), neurofilament (1:300, SMI-312, BioLegend), and stem cell antigen 1 (SCA1, AB4336, Millipore). Appropriate fluorochrome-conjugated secondary antibodies (1:100; A11037, A11029, or A-11055 from Invitrogen) were used as described previously.[1,3,5] Images were captured at 10×and 20×magnification using a Zeiss Axiocam microscope for qualitative analysis ($n = 3$ muscles/group).

All histology quantification was performed on full-size muscle sections by blinded investigators. Stained slides were scanned to obtain composite images of the entire muscle section using Olympus BX614S (Saint Louis University) and NanoZoomer 2.0 HT (Washington University in Saint Louis). Full-size muscle sections stained with H&E were used to quantify the number of myofibers with centrally located nuclei (CLN) at day 28 post-injury ($n = 5$ muscles/group). Full-size muscle sections stained with myosin heavy chain (MHC) and collagen (COL) were used to quantify the MHC:COL ratio by percentage area ($n = 4–5$ muscles/group). Images were opened in ImageJ (or Fiji) and the remaining defect area and remaining muscle tissue were divided into two separate images of the same size. The two images (i.e., one containing the defect area and the other containing the remaining healthy tissue), were separately analyzed by splitting the color channels, thresholding the MHC and COL to most accurately represent the stained area, and measuring the percentage of area positively stained by MHC and collagen. The percentage area of MHC and collagen from the two images were added up, and the MHC:COL ratio was determined. The muscle sections were split into remaining muscle tissue and defect area in order to measure the collagen deposition accurately. The collagen tissue deposited in the defect showed different sensitivity to thresholding than the collagen in the remaining healthy tissue. When thresholding without splitting, low thresholding results in the defect area not being picked up, whereas high thresholding results in collagen filling the muscle fibers. Thresholding the defect region and the remaining healthy tissue separately allowed for accurate detection and measurement of collagen (Supplemental Figure 1).

Muscle cross-sections were stained using antibodies from Developmental Studies Hybridoma Bank (Iowa City, IA, USA) for fiber types 1 (1:20; BA.D5), 2A (1:50; SC.71), and 2B (1:20; BF.F3), as described previously.[39] A laminin counterstain (1:100; ab11575) served as the fiber outline. Unstained fibers were identified as type 2X. Full-size muscle sections were scanned for analysis. A custom-designed image analysis MATLAB program was used for the quantification of myofiber cross-sectional area (CSA; $n = 5–6$ muscles/group) and fiber type distribution ($n = 5–6$ muscles/group). Briefly, the algorithm first thresholds the laminin channel, followed by nonlinear morphological transformations to delineate fiber boundaries and reduce noise. Area, circularity, and concavity filters are applied to identify myofibers. To avoid spatial variances in brightness, a color histogram is computed for each fiber, and areas corresponding to only a single channel are then compared to determine the primary fiber-type. If no color is dominant, the fiber is marked as 2X.

2.5 | Gene expression

As described previously,[5] RNA was isolated from snap-frozen cross-sections of TA muscle ($n = 4–5$ muscles/group) that was comprised of both the defect area and the remaining muscle mass (50 mg). RNA was extracted using Trizol LS reagent (Invitrogen) and purified using RNeasy mini kit (Qiagen). The yield of RNA was quantified using a NanoDrop spectrometer (NanoDrop Technologies) and optical density (OD) 260/280 ratios were determined. RNA (500 ng) was reverse transcribed into cDNA using the Super-Script III first-strand synthesis kit (Invitrogen). Custom designed primers (Sigma-Aldrich) with the sequences presented in Table 1 were used as myogenic and immunogenic markers. All primer sets have been synthesized by Sigma-Aldrich DNA oligos design tool. Aliquots (2 μl) of cDNA were amplified with 200 nM forward/reverse primers, SYBR GreenER (Invitrogen) in triplicate using a Bio-Rad CFX96 thermal cycler system (Bio-Rad). Non-template control and no reverse transcriptase controls were run for each reaction. Gene expression was normalized to 18S (housekeeping gene) to determine the ΔCT value. Expression levels for each mRNA transcript were determined by the $2^{-\Delta\Delta CT}$ method by normalizing each group to uninjured cage control muscles.

Additionally, gene expression of immunogenic markers was measured using a PCR immunoarray, as described previously.[40] RNA isolated as described above and was converted into complementary

TABLE 1 Primers used for qPCR

Gene	Forward sequence	Reverse sequence	Amplicon length, bp
Pax7	5′-GCAGTCGGACCACATTCAC-3′	5′-CGCACGACGGTTACTGAAC-3′	155
MyoD	5′-CGTGGCAGTGAGCACTACAG-3′	5′-TGTAGTAGGCGGCGTCGTA-3′	133
Myogenin	5′-CTACAGGCCTTGCTCAGCTC-3′	5′-GTTGGGACCAAACTCCAGTG-3′	153
eMHC	5′-TGGAGGACCAAATATGAGACG-3′	5′-CACCATCAAGTCCTCCACCT-3′	180
CTGF	5′-CAAGCAGCTGGGAGAACTG-3′	5′-ACAGGGTGCACCATCTTTG-3′	127
COL1	5′-CTGGTGAACGTGGTGCAG-3′	5′-GACCAATGGGACCAGTCAGA-3′	123
TGFB1	5′-GTCAGACATTCGGGAAGCA-3′	5′-CCAAGGTAACGCCAGGAAT-3′	138
18S	5′-GGCCCGAAGCGTTTACTT-3′	5′-ACCTCTAGCGGCGCAATAC-3′	173

DNA (cDNA) using RT^2 First Strand Kit (Qiagen). An RT^2 Profiler PCR array (PARN052Z, SABiosciences) was employed to examine rat innate and adaptive immune responses. A CFX96 Real-Time System (Bio Rad) was used to determine gene expression. Data analysis was carried out either with the online RT^2 Profiler PCR Array Data Analysis version 3.5 or expression levels for each mRNA transcript were determined by the $2^{-\Delta CT}$ method. Gene expression in VML-injured muscle tissue was relative to expression in uninjured cage control muscle tissue and normalized to reference gene Rplp1 ($n = 4$ muscles/group).

2.6 | Flow cytometry

Cells were isolated from the entire TA muscle with the muscle defect ($n = 4$–6 muscles per group) by enzymatic digestion as previously described.[37,40] Briefly, the TA was surgically isolated, and the mass was determined. Tissue was incubated with collagenase type II and dispase for 90 min at 37°C. Cells were further released by gentle mechanical disruption and filtered through a 70 μm cell strainer and subsequently through a 40 μm cell strainer. Erythrocytes were lysed with ammonium-chloride-potassium lysing buffer, and cells were washed and resuspended in Roswell Park Memorial Institute medium with 1% fetal bovine serum and 1% penicillin–streptomycin. Viable cells were quantified using trypan blue exclusion on a hemocytometer. After quantification, cells were resuspended at 10^6 cells/ml in PBS containing 0.5% FBS and 0.1% sodium azide. The resuspended cells were incubated with anti-CD32 antibody (BD Biosciences 550271) to block Fc receptors and labeled with monoclonal antibody cocktails to identify innate and adaptive immune cells in the VML injured muscles. The cells were labeled with anti-CD11b (BD Biosciences 562102, clone WT.5) and anti-CD3 (BD Biosciences 558493, clone IF4). Samples were run on BD biosciences LSR II flow cytometer at the flow cytometry research core facility at Saint Louis University. FlowJo software (BD Biosciences) was used for the analysis of flow cytometry data.

2.7 | Western blotting

TA muscles were cut axially at the defect site and the bottom portion was snap frozen in liquid nitrogen and stored at −20°C. TA muscle (40–60 mg) was homogenized in 500 μl of 1X RIPA lysis buffer (10× stock solution; 20–188; Millipore Sigma) and protease inhibitor cocktail (1:100, MilliporeSigma) on ice using a VWR 200 homogenizer (VWR, Radnor, PA) to isolate protein ($n = 6$ muscles per group). The protein concentrations were determined with the Pierce BCA protein assay kit (Thermo Scientific, Waltham, MA). Proteins were resolved by sodium dodecyl sulfate-polyacrylamide gel electrophoresis using 50 μg of total protein per sample on 4–20% Tris-glycine gels (Bio-Rad, Hercules, CA). Transfer was made onto nitrocellulose membranes, which were stained with Ponceau S to ensure equal loading, and subsequently blocked for 1 hr at room temperature in Tris-buffered saline containing 0.05% (vol/vol) Tween 20 (TBST) and 5% (wt/vol) nonfat dried milk. Membranes were then incubated overnight at 4°C in TBST containing 5% bovine serum albumin (BSA) and one of the following primary antibodies: SCA-1 (Abcam) or CD140a (Thermo Fisher Scientific) diluted 1:1,000. Membranes were rinsed three times with TBST for 5 min, and then incubated at room temperature for 1 hr in TBST containing 5% nonfat dried milk and the appropriate horseradish peroxidase-conjugated secondary antibody (1:1000, Invitrogen). Membranes were rinsed three times with TBST for 5 min before exposure to ECL reagents (Bio-Rad). The membranes were imaged using the Bio-Rad ChemiDoc (Bio-Rad). Quantification of band intensity was performed using Image J. Data were normalized to Ponceau[41] and used for quantitative analysis.

2.8 | Muscle function assessment

In vivo functional testing of the anterior crural muscles ($n = 7$–10 muscles/group) was performed at 28 days post-injury using the methodology previously described.[37] Briefly, in vivo physiological properties were measured in anesthetized rats (isoflurane 1.5–2.0%) using a dual-mode muscle lever system (Aurora Scientific, Inc., Mod. 305b). The skin was shaved, and an incision was made at the postero-lateral aspect of the ankle. The distal tendon of the gastrocnemius-soleus complex muscles was isolated and severed to prevent plantarflexion. Subcutaneous needle electrodes were inserted in the posterior compartment of the lower limb on each side of the common peroneal nerve. Optimal current (30–40 mA) was set with a series of twitches. Isometric tetanic contractions were elicited at 150 Hz (0.1 ms pulse width, 400 ms train) with the ankle at a right angle.

2.9 | Statistical analysis

Data are presented as a mean ± *SEM*. Analysis and graphing of data were performed using GraphPad Prism 8 for Windows. A one-way or two-way analysis of variance was used when appropriate to determine if there was a significant interaction or main effect between variables. The Fisher's least significant difference post-hoc comparison was performed to identify significance with $p < 0.05$. The PCR immunoarray data was analyzed using RT^2 Profiler PCR Array Data Analysis version 3.5. Western blotting data were analyzed using unpaired *t*-test.

3 | RESULTS

3.1 | FK-506 release

The amount of FK506 released from the sponges encapsulating 25 μM of FK-506 over 7 days is shown in Figure 1. The majority of the FK-506 loaded on to the sponges was released within the first 3 days, suggesting burst release of the encapsulated drug.

A PCR array was used to quantify gene expression of markers associated with innate and adaptive immune responses (Figure 1b). Out of the 84 genes analyzed, only the expression of pro-inflammatory cytokine interferon-gamma (IFN-γ) was significantly upregulated by 3.77-fold compared to the untreated group. However, the expression of interferon gamma receptor (IFN- γR1) and interleukin receptor (IL-1R1) was significantly downregulated by −2.13 and − 1.91-fold, respectively in the sponge treated group compared to the untreated group. The expression of cytotoxic T cell marker (CD8a) was found significantly downregulated (−1.96-fold) in sponge treated group compared to the untreated group. MX2 was significantly downregulated −11.52-fold in the sponge treated muscles compared to untreated muscles.

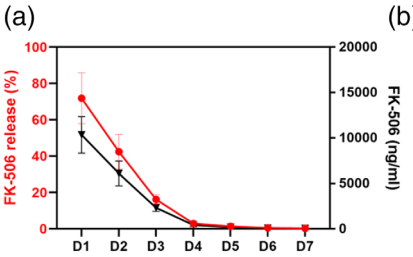

(b)

Upregulated

Gene	FC	p-value
TLR1	2.31	0.4555
TLR5	4.3	0.2047
TLR6	2.07	0.119
TLR9	2.68	0.1747
NLRP3	2.57	0.2528
C3	3.41	0.2982
CCR6	4.25	0.4721
IFN-γ	3.77	0.0079*
CD4	2.34	0.9546

Downregulated

Gene	FC	p-value
CAMP	-2.16	0.4019
CXCR3	-2.01	0.6983
CXCL10	-2.01	0.3621
CCL3	-2.87	0.8159
IL-13	-2.25	0.4327
IL1-R1	-2.13	0.0129*
IFN-γR1	-1.91	0.0287*
CD40	-3.84	0.0734
FOXP3	-3.96	0.112
CD8A	-1.96	0.0149*
FasLg	-2.14	0.6161
CASP1	-8.42	0.9812
STAT6	-23.04	0.1496
MX2	-11.52	0.0301*
IRF7	-3.94	0.2858

FIGURE 1 (a) FK506 release from biomimetic sponges was measured in vitro. The percentage release is plotted on the left y-axis (red circles) while the concentration of the released drug is plotted on the right y-axis (black triangles) (b) An array of immunogenic markers was quantified via PCR. The table shows genes found downregulated and upregulated within sponge-treated muscles compared to untreated muscles. FC, fold change

3.2 | Cellular infiltration

On Day 7, qualitative analysis of the cellular infiltration showed that while T cells ($CD3^+$) remained around the periphery, the macrophages ($CD68^+$) infiltrated the three-dimensional structure of the sponges (Figure 2). Quantitative analysis of mononuclear cell infiltration was performed using flow cytometry at Days 7, 14, and 28 post-injury. Cells isolated from the TA muscles were gated for T cells ($CD3^+$) and myeloid cells ($CD11b^+$). While both T cells and myeloid cells were elevated in response to VML injury, no statistical differences were observed between untreated and treated experimental groups. We did not stain for $CD11b^+$ myeloid subsets (i.e., neutrophils, macrophages, dendritic cells etc.) in this study. However, a majority (~75–80%) of the infiltrating $CD11b^+$ cells have been previously identified as monocytes or macrophages in a cardiotoxin induced muscle injury model.[42]

On Day 7, both untreated and treated muscles supported endothelial cells ($CD31^+$) and stem cell ($SCA1^+$) infiltration in the VML defect region (Figure 3a,b). Quantification of SCA-1 expression by western blotting trended toward an increase ($p = 0.0768$) in treated samples on Day 7 (Figure 3c). The expression of CD140a (or PDGFRα)-a marker associated with fibroadipogenic progenitor cells[43] showed no statistical differences between the treated and untreated samples ($p = 0.1192$) on Day 7 (Figure 3d).

3.3 | Muscle mass and function

TA muscle mass was significantly lower in the VML injured muscles irrespective of treatment on Days 7, 14, and 28 post-injury compared to the uninjured controls (Figure 4a). A > 35% deficit in muscle mass was observed between uninjured controls and VML injured muscles over 28 days. No significant differences were observed between untreated and treated muscles at any time-points.

The isometric strength of the anterior crural muscles was measured in vivo at 28 days post-injury. VML injury resulted in a ~ 56–59% deficit in peak isometric torque production when analyzing raw force data and that normalized to body mass (Table 2). Sponge treatment significantly improved the torque production in VML injured muscles (Figure 4b-d)). Compared to untreated muscles, biomimetic sponges improved muscle strength by ~31–37% when analyzing raw force data and that normalized to body mass or TA muscle mass. Histological analysis of acetylcholine receptor clusters co-localized with

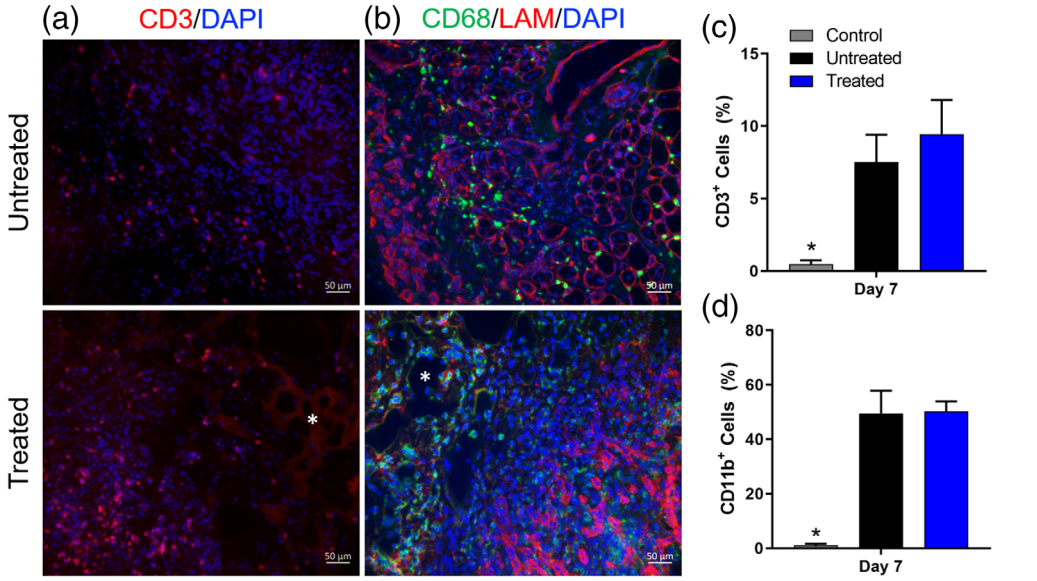

FIGURE 2 Muscle cross-sections were stained for (a) T cells (CD3) and (b) macrophages (CD68) on Day 7. The percentage of (c) $CD3^+$ T cells and (d) $CD11b^+$ myeloid cells was quantified using flow cytometry on Day 7

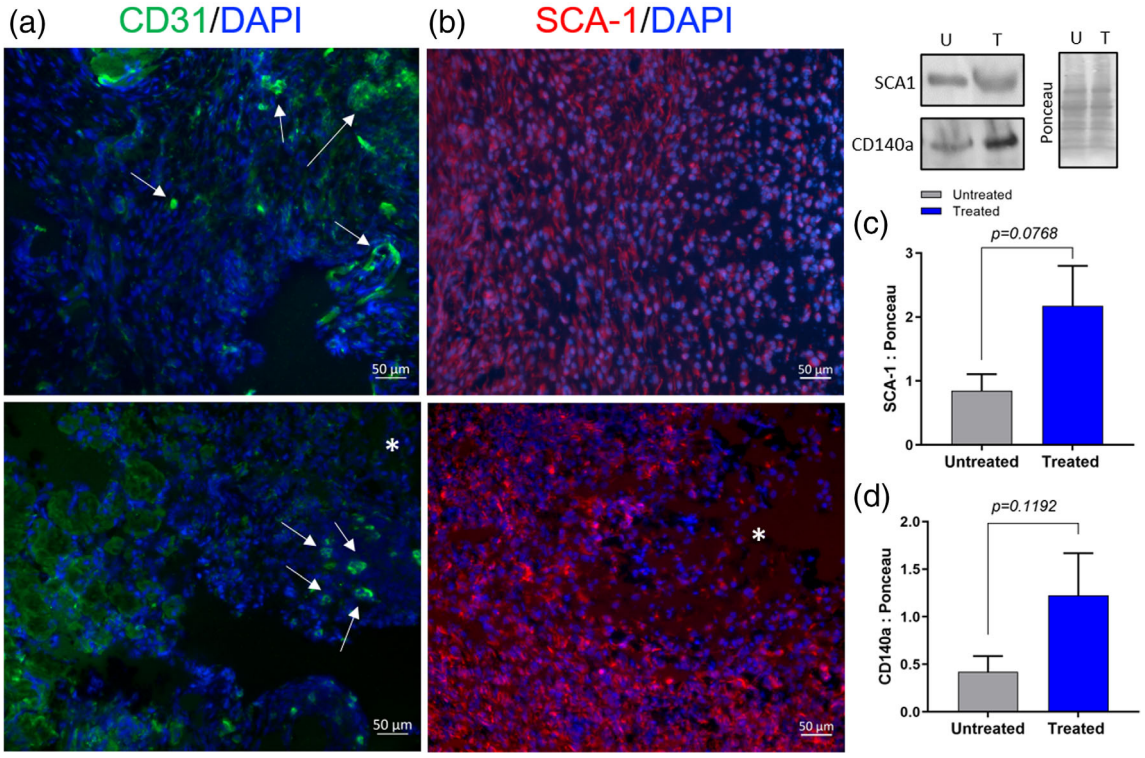

FIGURE 3 Muscle cross-sections were stained for (a) endothelial cells (CD31), and (b) stem cells (SCA-1) on Day 7. The white asterisk indicates the implanted sponge in the defect and white arrows indicate some $CD31^+$ cells in the defect. The protein expression of (c) SCA-1 and (d) CD140a on Day 7 was quantified using western blotting

neurofilament revealed no differences in muscle innervation between untreated and treated muscles (Figure 4e).

3.4 | Myofiber regeneration and fibrosis

Transverse cross-sections of TA muscles were stained with H&E and are shown in Figure 2. On Day 7, the implanted sponges can be identified in the VML defect. The sponges appear to support cellular infiltration and do not cause fibrotic capsule formation. By Day 14, the sponges are no longer visible in the defect. On Day 28, quantitative analysis revealed that there are significantly more myofibers with CLN in treated muscles versus untreated muscles (Figure 5).

Muscle cross-sections were also stained with myosin heavy chain (MHC) and collagen (COL), as shown in Figure 6. At all three time-points, increased cellular infiltration ($DAPI^+$) can be observed in the

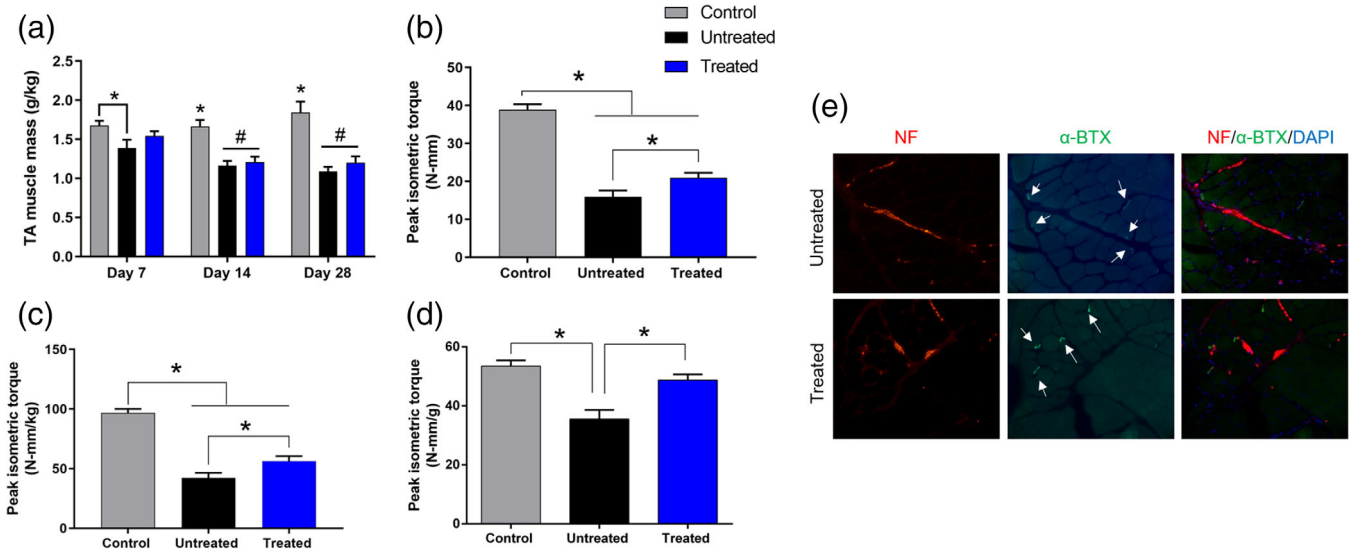

FIGURE 4 Biomimetic sponge enhances muscle function but not muscle mass following volumetric muscle loss (VML) injury. (a) Tibialis anterior muscles were weighed upon collection at Days 7, 14, and 28 post-injury. (b) Peak isometric torque was measured and (c) normalized to body weight and (d) TA weight. (e) Qualitative analysis of injured muscles showed no differences in the prevalence of colocalized pre- and post-synaptic terminals. "*" indicates a statistical difference ($p < 0.05$) between different treatment groups at a particular time-point. "#" indicates a statistical difference ($p < 0.05$) from Day 7 for a particular treatment group. White arrows indicate positively stained acetylcholine receptor clusters. NF, neurofilament, α-BTX, alpha-bungarotoxin

TABLE 2 Extent of functional recovery following VML injury

		4 weeks post-injury		
		Uninjured	Injured	
Parameters		Cage control	Untreated	Treated
Unnormalized	Peak isometric torque (N-mm)	38.91	15.90	20.90
	Functional deficit (%)		59.14	46.29
	Functional recovery (%)			31.45
Normalized to body weight	Peak isometric torque (N-mm/kg)	96.87	42.19	56.30
	Functional deficit (%)		56.45	41.88
	Functional recovery (%)			33.44
Normalized to TA weight	Peak isometric torque (N-mm/g)	53.46	35.53	48.75
	Functional deficit (%)		33.54	8.81
	Functional recovery (%)			37.21

Abbreviation: VML, volumetric muscle loss.

defect site. On Day 7, both untreated and treated muscles showed a large defect region filled with collagenous fibrotic tissue. The remodeled sponge could be identified in the defect. On Day 14, the untreated muscles continued to show collagenous fibrotic tissue deposition. However, in the sponge treated muscles, the defect region appeared smaller with less fibrotic tissue. Several small diameter MHC^+ myofibers could also be identified in the defect region of the sponge treated muscles (Supplemental Figure 2). By Day 28, the sponge treated muscles continued to show a smaller fibrotic region as well as increased presence of MHC^+ myofibers in and around the defect region. Muscle regeneration and fibrosis was assessed by analyzing the ratio of myosin heavy chain to collagen (MHC: COL). The MHC:COL ratio was statistically similar between the untreated and sponge treated muscles on Day 7. On Day 14, sponge treated muscles trended toward an increased MHC:COL ratio ($p = 0.055$), and on Day 28, the sponge treated muscles showed statistically higher MHC:COL ratio compared to the untreated muscles.

3.5 | Myogenic marker expression

Gene expression of myogenic markers is shown in Supplementary Figure 2. Pax7 and MyoD are markers associated with satellite cell activation and proliferation. Irrespective of treatment, Pax7 shows a

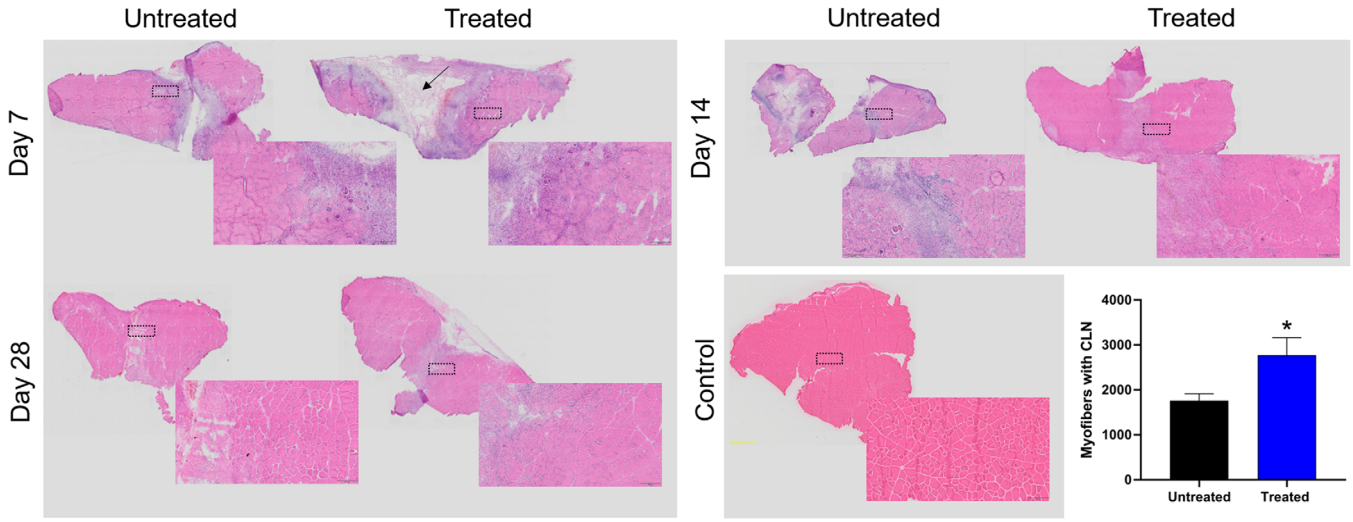

FIGURE 5 Transverse muscle cross-sections were stained with H&E and whole slide images were captured at Days 7, 14, and 28 post-injury. The defect area in the injured muscles can be identified as the region with high density of nuclei. Treated muscles had more myofibers with centrally located nuclei (CLN) at Day 28. "*" indicates a statistical difference ($p < 0.05$) between different treatment groups. The black arrow indicates the sponge in the defect. The dashed black rectangles approximate the area of the muscle section that is shown magnified (scale bar = 200 μm)

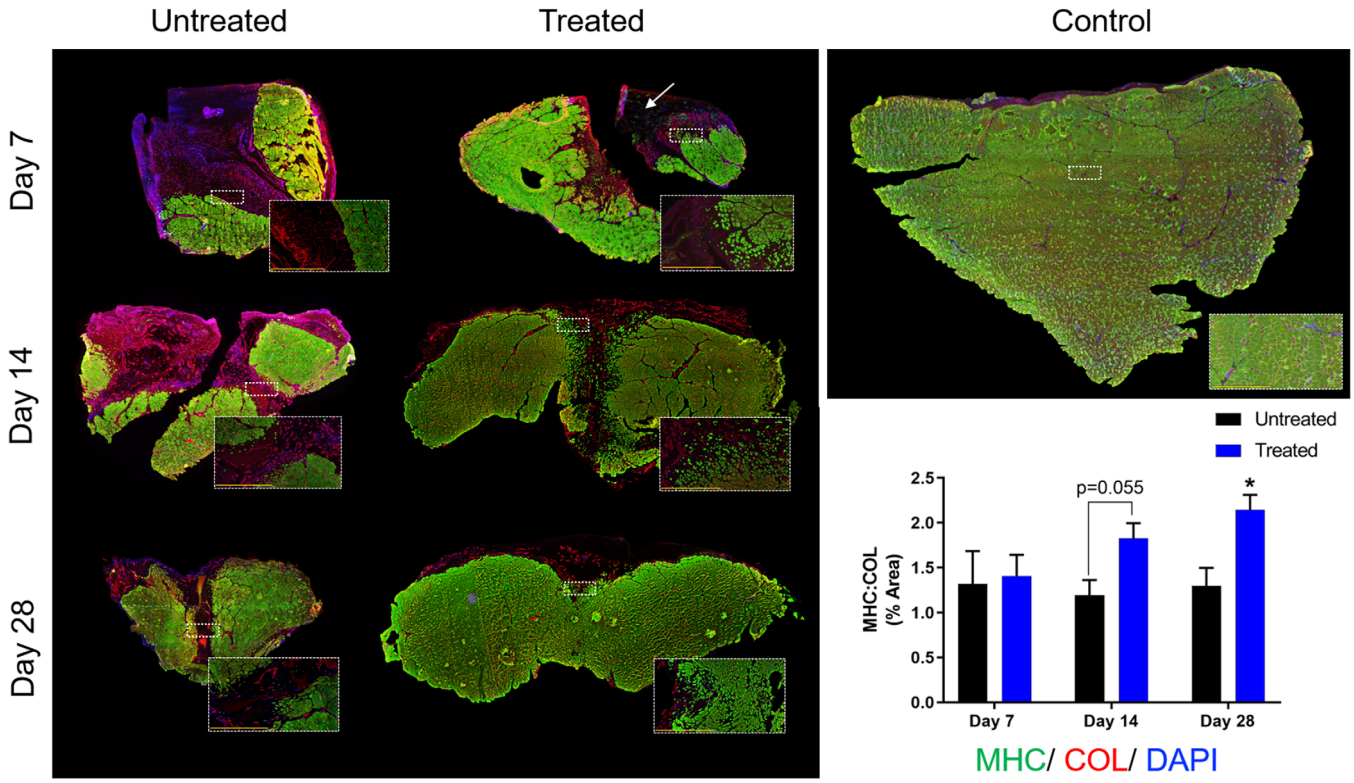

FIGURE 6 Transverse muscle cross-sections were stained with myosin heavy chain (MHC), collagen (COL), and DAPI. The percentage (%) area of MHC and COL were quantified and MHC:COL ratios were calculated. Treated muscles have higher MHC:COL ratios by Day 28 post-injury. "*" indicates a statistical difference ($p < 0.05$) between different treatment groups at a particular time-point. The white arrow indicates the sponge in the defect. The dashed white rectangles approximate the area of the muscle section that is shown magnified (scale bar = 800 μm)

transient decrease on Day 14 followed by an increase on Day 28. MyoD expression shows an increase between Days 7 and 28 in both treated and untreated samples. Although not significant, myogenin expression is higher with sponge treatment on Day 7. Similar to Pax7, it also shows a transient drop at Day 14 followed by an increase at the Day 28 time-point, but only in the sponge treated group. In the

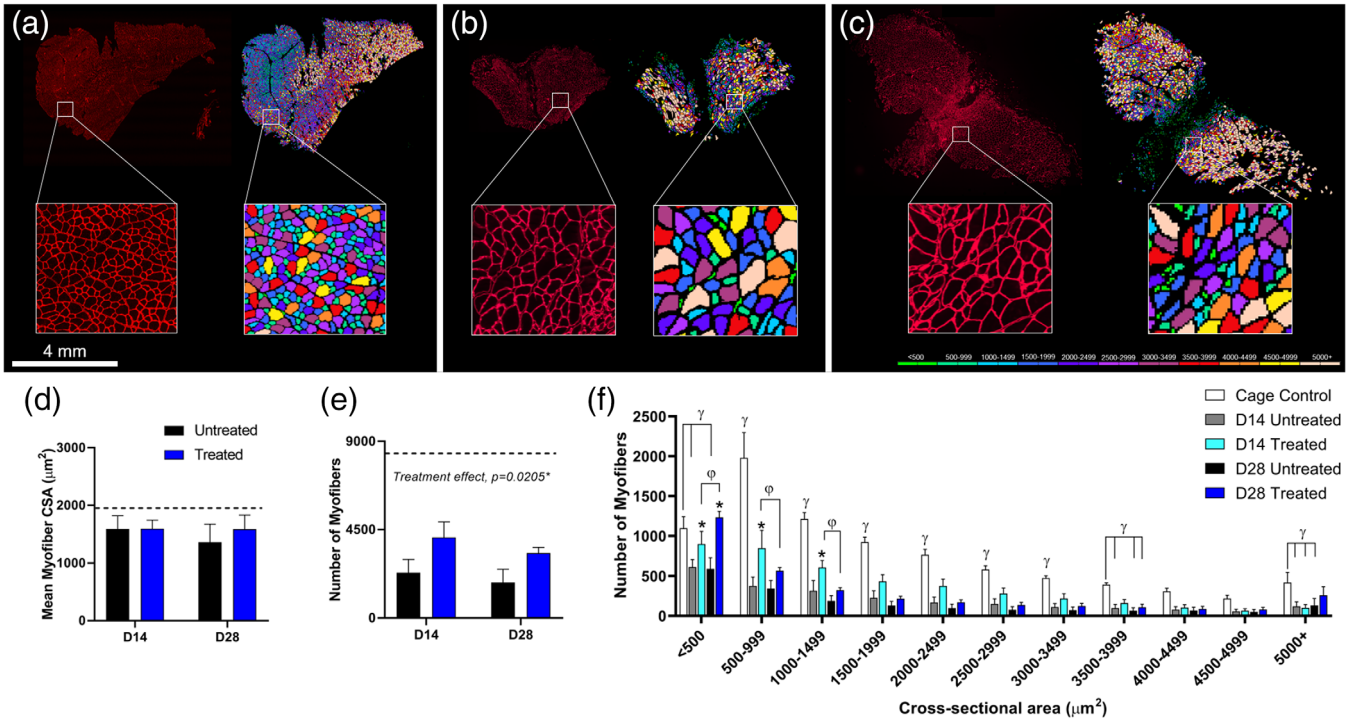

FIGURE 7 Muscle fibers were outlined with laminin and cross-sectional areas were quantified. Myofiber cross sectional area (CSA) at Day 28 for (a) cage control, (b) untreated, and (c) treated groups are displayed as color-coded maps. (d) A higher quantity of small CSA fibers (<500 μm^2) were present in treated muscles at both Days 14 and 28 post-injury. (e) Treated muscles also contained higher numbers of total myofibers than untreated muscles at Days 14 and 28. (f) The mean CSA was not different between untreated and treated groups. "*" indicates a statistical difference ($p < 0.05$) between untreated and treated muscles at a particular time-point. "γ" indicates a statistical difference ($p < 0.05$) between controls and injured muscles at a particular time-point. "φ" indicates a statistical difference ($p < 0.05$) between Day 14 and 28 for a particular treatment group. The dashed line indicates the value for the control sample

untreated group, myogenin expression does not show any significant differences over-time. Embryonic myosin heavy chain (eMHC) maintains its expression over 14 days in the sponge treated group. However, it shows a sharp decline in the untreated groups. eMHC expression was higher in the sponge treated group compared to the untreated group at Day 14, but statistical significance was not reached. On day 28, the expression of eMHC is significantly lower than Day 7 in both treatment groups.

A trend toward increased TGF-β1 expression is observed with sponge treatment. On Days 14 and 28, both treated and untreated muscles show significantly reduced TGF-β1 expression compared to Day 7. Collagen 1 gene expression is significantly reduced on Days 14 and 28 in the untreated muscles.

3.6 | CSA measurement

Laminin stained muscle cross-section used for CSA analysis are shown in Figure 7(a)-c. The mean CSA was statistically similar between the untreated and treated muscles (Figure 7d). The total number of myofibers in the cage control TA muscle cross-sections were determined to be 8,374 ± 937 (mean ± *SD*). VML injury reduced the total number of myofibers in the TA muscle by ~78% on Day 14 (Figure 7 (e)). On both Days 14 and 28, sponge treatment significantly increased the total number of myofibers (treatment effect, $p = 0.0205$). The percentage improvement in the number of myofibers with sponge treatment was 77 and 82%, on Days 14 and 28, respectively. Sponge treatment significantly increased the number of small diameter myofibers (<500 μm^2) on both Days 14 and 28 post-VML injury (Figure 7f). The number of fibers in the CSA range of 500–999 μm^2 and 1,000–1,499 μm^2 were also significantly higher with sponge treatment on Day 14 post-VML. The number of small diameter fibers (<500 μm^2) showed a significant increase from Day 14 to Day 28 in the sponge treated groups. A simultaneous decline in the number of bigger fibers (500–1,500 μm^2) was observed with sponge treatment on Day 28 compared to Day 14.

Fiber type specific CSA analysis revealed no change in the percentage of either Type 1, 2A, 2B or 2X myofibers with VML injury (Figure 8d). However, the mean CSA of fast-twitch glycolytic fibers (i.e., type 2B and 2X) was significantly lower with VML injury (Figure 8e). Sponge treated muscles showed significantly larger CSA of type 2B myofibers compared to untreated muscles. Fiber type distribution analysis (Figure 8f-I) showed that sponge treatment significantly increased the number of small diameter fibers (<500 μm^2) in the slow oxidative fibers (i.e., type 1 and 2A), and large-diameter myofibers (>4,000 μm^2) in the fast-twitch type 2B fibers.

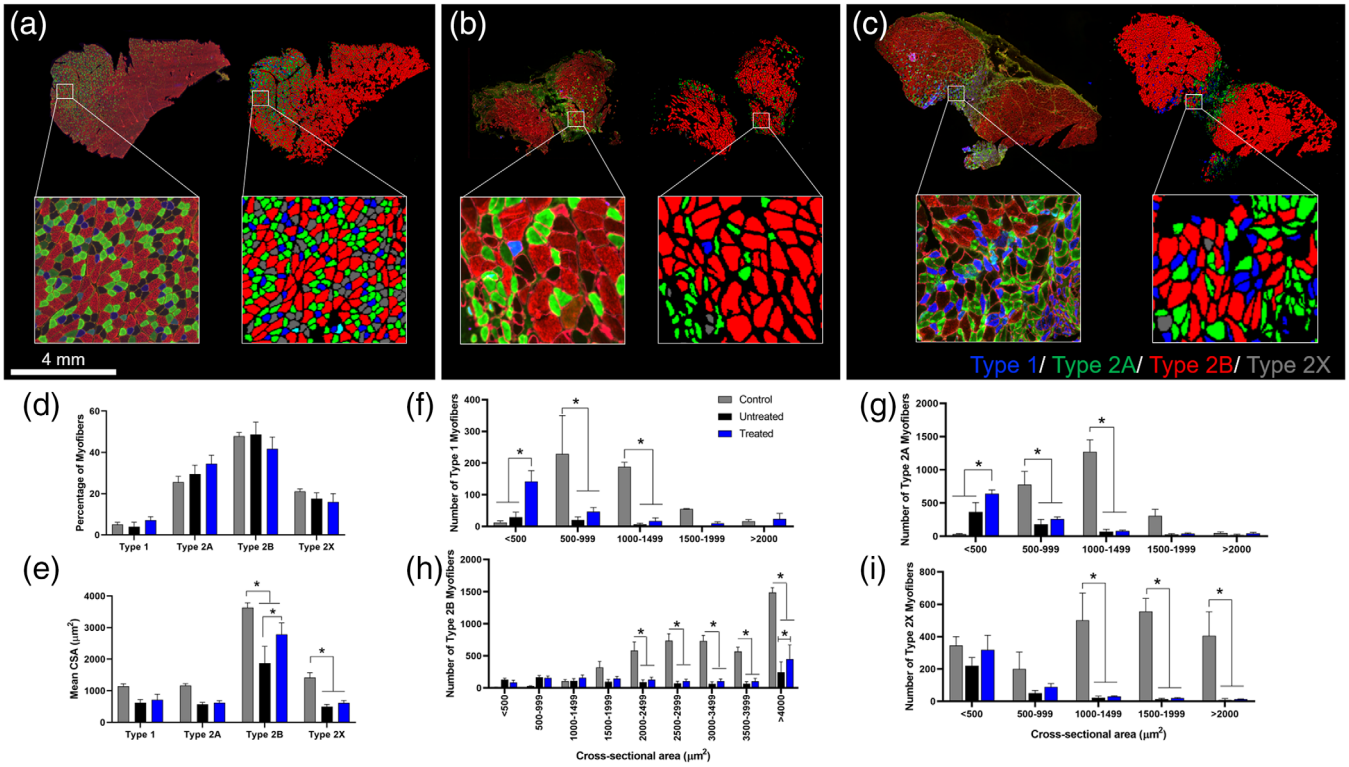

FIGURE 8 Muscle cross-sections were stained for different fast- and slow- twitch fiber types. Immunostained images and color-coded maps are displayed for (a) uninjured controls, (b) untreated muscles, and (c) sponge-treated muscles. Fiber type distribution and CSA was quantified. (d) volumetric muscle loss (VML) had no effect on the percentages of different types of fibers, but (e) decreased the mean cross sectional area (CSA) of fast-twitch fibers (i.e., type 2B and 2X). Sponge treatment increased the mean CSA of Type 2B fibers compared to untreated muscles. Fiber type CSA distributions for (f) Type 1, (g) Type 2A, (h) Type 2B, and (i) Type 2X myofibers are shown. "*" indicates a statistical difference ($p < 0.05$) between different treatment groups

4 | DISCUSSION

The most important finding of this study is that FK-506 loaded biomimetic sponges improve muscle structure and function in a rodent model of VML. Sponge treatment significantly increased the number of total and regenerating myofibers, type 2B fiber CSA, MHC: COL ratio, and muscle function compared to untreated VML injured muscles. These results are encouraging, and we believe that biomimetic sponges may provide a promising "off-the-shelf" approach for VML that is worthy of clinical investigation.

An increase in the number of myofibers and type 2B fiber CSA may underlie the basis for improved muscle function with sponge treatment. To the best of our knowledge, significant increases in myofiber number, mean type 2B CSA, and muscle function have never been reported with the implantation of an acellular ECM scaffold in a full-thickness VML model. In some previous studies, improvement in muscle regeneration following injury has only been reported when acellular ECM scaffolds have been combined with stem cells,[42] minced muscle grafts,[43] or growth factors.[44] The use of decellularized scaffolds in VML injuries have shown conflicting results with studies reporting either no improvement,[42,45,46] exacerbated force deficits,[47] or modest improvements in force production.[48] While scaffolds that contain myogenic stem cells have shown improvement in muscle regeneration and force production,[5,49-51] their clinical translation is likely to be hindered by limited availability of autologous donor tissue and potential donor-site morbidity.

In this study, the biomimetic sponges were expected to stimulate muscle regeneration while limiting the extent of inflammation and fibrosis. The sponges contain ECM proteins such as gelatin, collagen, and LA-111, and have supported myogenic activity in vitro and in vivo in a previous study.[33] Besides FK-506, immunomodulatory and anti-inflammatory effects can also be ascribed to ECM scaffolds.[52] While it is difficult to attribute specific immunomodulatory or regenerative effects to the different constituents of biomimetic sponges, our results suggest that their implantation modulated the VML microenvironment in a way that improved muscle structure and function.

To gain further insight into the immune response within the first 7 days post-injury, we performed a PCR immunoarray. Out of the 84 genes analyzed, sponge treatment resulted in significant upregulation of only IFN-γ. The primary producers of IFN-γ are activated T cells. It is an inflammatory cytokine that regulates various immune responses inducing macrophage activation.[53-55] A study reported that IFN-γ null mice show impaired muscle healing associated with decreased macrophage function and increased fibrosis.[53] It has also been shown that exogenous IFN-γ can reduce fibrosis and support muscle cell proliferation and differentiation.[54] Cytokine

receptors IL-1R and IFN-γR1 were found significantly downregulated with sponge treatment. Several immune cells express IL-1R and IFN-γR1 and some studies have also suggested that myofibers express these receptors as well.[56,57] Downregulation of the receptors, IL-1R and IFN-γR1, on immune cells and myofibers likely indicates suppressed responsiveness to the effect of pro-inflammatory cytokines. In this work MX2, which encodes the protein MxB, was significantly reduced by sponge treatment. MX2 is known to be an interferon-induced gene, particularly by the innate type I interferons.[58] While IFN-γR1 indicates a later, more adaptive response of type II interferon, this concordance of reduced expression is evidence of potential suppression of an overall interferon response at the site of injury. Further supporting this analysis, is a study that reported ligand-independent downregulation of IFN-γR1 on activated T-cells with cyclosporine A,[59] a drug with similar mechanism of action to FK-506. However, more studies are needed to substantiate this claim.

Sponge treatment significantly downregulated the gene expression of cytotoxic T cell marker (CD8a) on Day 7 post-injury. T cells play complex roles in skeletal muscle regeneration and show varied responses to muscular dystrophies and injuries. Pathological muscle conditions such as Duchenne Muscular Dystrophy are characterized by the increased and persistent presence of $CD8^+$ T –cells.[60] Studies have suggested that $CD8^+$ T cells could have a direct cytotoxic role on muscle fibers expressing major histocompatibility complex (MHC) class I molecules.[61] Healthy individuals do not show MHC class I myofibers, but they are frequently observed in myositis patients. In another study, depletion of $CD8^+$ T cells in cardiotoxin damaged Casitas B-lineage lymphoma-b (Cbl-b)-deficient mice resulted in improved regenerative outcomes.[62]

In contrast, other studies have indicated that T cells might play a role in muscle regeneration, and completely abolishing T cell response could have detrimental effects. For instance, in a model of cardiotoxin induced muscle injury, it was observed that in the absence of $CD8^+$ T cells, matrix deposition is increased. At the same time, monocyte recruitment, myoblast proliferation, and myofiber growth are diminished.[63] In a study by Hurtgen et al., implantation of minced muscle autografts resulted in enhanced presence of $CD3^+$, $CD4^+$, and $CD8^+$ T cells in a VML model.[64] The increased presence of these cell types over 14 days post-injury did not hinder muscle regeneration, as evidenced by newly regenerating myofibers and improved functional recovery. In a human study, increased presence of $CD8^+$ T cells was implicated in muscle adaptation to repeated eccentric contractions.[65,66] The fact that $CD8^+$ T cells were increased significantly only after second bout of exercise when evidence of muscle damage was reduced, suggested that these cells do not exacerbate injury but facilitate repair.[56,65] Therefore, the exact mechanism through which $CD8^+$ T cells participate in muscle regeneration following VML remains unknown and needs to be investigated in future studies.

Interestingly, we did not observe heightened myogenic gene expression with sponge treatment of VML injury. However, we observed a significantly higher number of total and small diameter myofibers (<500 μm^2) as well as myofibers with CLN following sponge treatment, which would be indicative of increased myofiber regeneration. We believe that myofiber splitting could account for the significant increase in the small diameter myofibers on Days 14 and 28 in the sponge treated muscles.[67] Qualitative analysis showed several myofibers with irregular shapes and displaced myonuclei, from which a smaller myofiber appeared to have broken apart. Myofiber splitting has been observed in hypertrophy models,[68] which indicates that the process may be an adaptation to maintain either the myonuclear domain, oxygen diffusion capacity, or force production.[69] In VML models, the remaining muscle mass experiences chronic overload as it attempts to compensate for the lost tissue.[8] It has been suggested that myofiber splitting in response to increased loading can be biomechanically advantageous as it distributes the force over a larger surface area.[69] Therefore, myofiber splitting may account for higher myofiber counts and peak isometric torque in sponge treated muscles. Future studies will investigate the extent of myofiber splitting in VML injured muscles.

We have also demonstrated that VML injury primarily impacts the CSA of fast glycolytic fibers (i.e., Type 2B and 2X). This result is in agreement with previous studies where eccentric contractions,[70] DMD,[71] and aging[72] were shown to impact type 2 fibers selectively. In a previous study, a ~ 20% VML defect resulted in chronic axotomy of ~69% of the motor-neurons innervating that muscle.[73] In this study, we did not observe a change in the overall percentage of myofiber types at the Day 28 time-point. But it is possible for the denervated fast fibers to be reinnervated by slow motor units at later time-points, causing an increase in the distribution of slow oxidative fibers (i.e., Type I and 2A) in the VML injured muscles.[74]

In this study, the sponge treated muscles showed several clusters of small-diameter myofibers, the majority of which appeared to be Type 1 or 2A myofibers. Quantitative analysis also confirmed significantly higher numbers of small diameter myofibers (<500 μm^2) in the fiber type 1 and 2A category. Sponge treatment partially rescued the CSA of type 2B but not 2X myofibers. Sponge treated muscles showed significantly higher CSA of type 2B myofibers as well as greater number of large diameter (> 4,000 μm^2) type 2B fibers compared to untreated VML injured muscles. An improvement in type 2B myofiber CSA could also account for increased force production. These findings have major implications for VML injured patients because large type 2B fibers can withstand substantial loads. Therefore, preventing their loss and preserving their CSA might help improve the quality of life in affected patients.[75]

We did not investigate the in vivo release kinetics of FK-506, but it can be reasonably assumed that this hydrophobic small-molecule is cleared within the first few days after sponge implantation in the VML injured muscle. Interestingly, it has been shown that dendritic cells can sequester FK-506 and release it slowly in quantities that can inhibit T cell activity for at least 72 hr.[76] Dendritic cells have been detected as early as 24 hr after muscle injury.[77,78] While continuous administration of FK-506 has been done in VML models,[37,79] others have reported that a single local application of FK-506 at the time of repair can support functional nerve regeneration 2–3 months after injury.[80,81] If desired, prolonged immunomodulation can be easily achieved in a clinical setting by administering FK-506 either as an oral

dose or intravenous infusion.[82] Another limitation of the study is the lack of a control group treated with sponge without FK-506. The efficacy of FK-506 in VML models has been well-established in previous studies.[37,79] We compared our material to the untreated VML control because majority of the VML injuries are left untreated in a clinical setting,[40,83] as there are no FDA approved regenerative treatments.

Despite the promising results reported in this study, significant challenges remain in restoring muscle mass and function following VML. Further testing is required to identify the specific contribution of biomimetic sponges and FK-506 towards muscle regeneration and function following VML. Future work will also investigate the extent to which functional recovery can be enhanced by combining biomimetic sponge treatment with bioactive factors and physical rehabilitation.[84]

5 | CONCLUSION

Overall, these results suggest that biomimetic sponges integrate well with the surrounding muscle tissue around the VML defect and support cellular infiltration. Biomimetic sponge treatment reduces the severity of the VML injury and allows for improvements in muscle structure and function. These results could be attributed to the replenishment of vital ECM proteins, immunomodulation, and mechanical support offered by the three-dimensional scaffold at the site of VML injury.

ACKNOWLEDGMENTS

This work was supported by a grant from the National Institute of Health (NIGMS) 1R15GM129731 awarded to Koyal Garg. We would like to thank Gary D. London (Washington University), as well as Caroline Murphy and Dr. Grant Kolar (Saint Louis University) for technical assistance with histological imaging. We would like to thank the Flow Cytometry Core Facility at Saint Louis University and Joy Eslick as well as Sherri Koehm for technical assistance with data acquisition and analysis.

CONFLICT OF INTEREST

Koyal Garg has equity interest in GenAssist, Inc., and serves on the company's scientific advisory board. GenAssist, Inc. is developing products related to the research described in this paper. The terms of this arrangement have been reviewed and approved by Saint Louis University, in accordance with its conflict of interest policies. GH (Gabriel Haas) is the CEO and Josh Madsen is the CTO of GenAssist, Inc. and both are members of the board of directors. AD (Andrew Dunn) also holds equity interest in GenAssist, Inc.

DATA AVAILABILITY STATEMENT

The data that support the findings of this study are available from the corresponding author upon reasonable request.

REFERENCES

1. Garg K, Ward CL, Rathbone CR, Corona BT. Transplantation of devitalized muscle scaffolds is insufficient for appreciable de novo muscle fiber regeneration after volumetric muscle loss injury. *Cell Tissue Res*. 2014;*358*(3):857-873.
2. Garg K, Ward CL, Hurtgen BJ, et al. Volumetric muscle loss: persistent functional deficits beyond frank loss of tissue. *J Orthop Res*. 2015;*33*(1):40-46.
3. Garg K, Corona BT, Walters TJ. Losartan administration reduces fibrosis but hinders functional recovery after volumetric muscle loss injury. *J Appl Physiol (1985)*. 2014;*117*(10):1120-1131.
4. Greising SM, Rivera JC, Goldman SM, Watts A, Aguilar CA, Corona BT. Unwavering pathobiology of volumetric muscle loss injury. *Sci Rep*. 2017;*7*(1):13179.
5. Corona BT, Garg K, Ward CL, McDaniel JS, Walters TJ, Rathbone CR. Autologous minced muscle grafts: a tissue engineering therapy for the volumetric loss of skeletal muscle. *Am J Physiol Cell Physiol*. 2013;*305*(7):C761-C775.
6. Bianchi B, Copelli C, Ferrari S, Ferri A, Sesenna E. Free flaps: outcomes and complications in head and neck reconstructions. *J Craniomaxillofac Surg*. 2009;*37*(8):438-442.
7. Urken ML, Weinberg H, Buchbinder D, et al. Microvascular free flaps in head and neck reconstruction. Report of 200 cases and review of complications. *Arch Otolaryngol Head Neck Surg*. 1994;*120*(6):633-640.
8. Aurora A, Garg K, Corona BT, Walters TJ. Physical rehabilitation improves muscle function following volumetric muscle loss injury. *BMC Sports Sci Med Rehabil*. 2014;*6*(1):41.
9. Garg K, Boppart MD. Influence of exercise and aging on extracellular matrix composition in the skeletal muscle stem cell niche. *J Appl Physiol (1985)*. 2016;*121*(5):1053-1058.
10. Dunn A, Talovic M, Patel K, Patel A, Marcinczyk M, Garg K. Biomaterial and stem cell-based strategies for skeletal muscle regeneration. *J Orthop Res*. 2019;*37*(6):1246-1262.
11. Larouche J, Greising SM, Corona BT, Aguilar CA. Robust inflammatory and fibrotic signaling following volumetric muscle loss: a barrier to muscle regeneration. *Cell Death Dis*. 2018;*9*(3):409.
12. Garg K, Corona BT, Walters TJ. Therapeutic strategies for preventing skeletal muscle fibrosis after injury. *Front Pharmacol*. 2015;*6*:87.
13. Aguilar CA, Greising SM, Watts A, et al. Multiscale analysis of a regenerative therapy for treatment of volumetric muscle loss injury. *Cell Death Discov*. 2018;*4*:33.
14. Garg K, Ward CL, Corona BT. Asynchronous inflammation and myogenic cell migration limit muscle tissue regeneration mediated by a cellular scaffolds. *Inflamm Cell Signal*. 2014;*1*(4):e530.
15. De Lisio M, Jensen T, Sukiennik RA, Huntsman HD, Boppart MD. Substrate and strain alter the muscle-derived mesenchymal stem cell secretome to promote myogenesis. *Stem Cell Res Ther*. 2014;*5*(3):74.
16. Goudenege S, Lamarre Y, Dumont N, et al. Laminin-111: a potential therapeutic agent for Duchenne muscular dystrophy. *Mol Ther*. 2010;*18*(12):2155-2163.
17. Rooney JE, Gurpur PB, Burkin DJ. Laminin-111 protein therapy prevents muscle disease in the mdx mouse model for Duchenne muscular dystrophy. *Proc Natl Acad Sci U S A*. 2009;*106*(19):7991-7996.
18. Rooney JE, Gurpur PB, Yablonka-Reuveni Z, Burkin DJ. Laminin-111 restores regenerative capacity in a mouse model for alpha7 integrin congenital myopathy. *Am J Pathol*. 2009;*174*(1):256-264.
19. Rodriguez IA, Sell SA, McCool JM, Saxena G, Spence AJ, Bowlin GL. A preliminary evaluation of lyophilized gelatin sponges, enhanced with platelet-rich plasma, hydroxyapatite and chitin whiskers for bone regeneration. *Cell*. 2013;*2*(2):244-265.
20. Hiwatashi N, Hirano S, Mizuta M, et al. Biocompatibility and efficacy of collagen/gelatin sponge scaffold with sustained release of basic fibroblast growth factor on vocal fold fibroblasts in 3-dimensional culture. *Ann Otol Rhinol Laryngol*. 2015;*124*(2):116-125.
21. Takemoto S, Morimoto N, Kimura Y, et al. Preparation of collagen/gelatin sponge scaffold for sustained release of bFGF. *Tissue Eng Part A*. 2008;*14*(10):1629-1638.

22. Ponticiello MS, Schinagl RM, Kadiyala S, Barry FP. Gelatin-based resorbable sponge as a carrier matrix for human mesenchymal stem cells in cartilage regeneration therapy. *J Biomed Mater Res*. 2000;*52*(2):246-255.
23. Imani R, Rafienia M, Hojjati Emami S. Synthesis and characterization of glutaraldehyde-based crosslinked gelatin as a local hemostat sponge in surgery: an in vitro study. *Biomed Mater Eng*. 2013;*23*(3):211-224.
24. Rohanizadeh R, Swain MV, Mason RS. Gelatin sponges (Gelfoam) as a scaffold for osteoblasts. *J Mater Sci Mater Med*. 2008;*19*(3):1173-1182.
25. Ju YM, Atala A, Yoo JJ, Lee SJ. In situ regeneration of skeletal muscle tissue through host cell recruitment. *Acta Biomater*. 2014;*10*(10):4332-4339.
26. Doi K, Ikeda T, Marui A, et al. Enhanced angiogenesis by gelatin hydrogels incorporating basic fibroblast growth factor in rabbit model of hind limb ischemia. *Heart Vessels*. 2007;*22*(2):104-108.
27. Okano T, Matsuda T. Hybrid muscular tissues: preparation of skeletal muscle cell-incorporated collagen gels. *Cell Transplant*. 1997;*6*(2):109-118.
28. Choi JS, Lee SJ, Christ GJ, Atala A, Yoo JJ. The influence of electrospun aligned poly(epsilon-caprolactone)/collagen nanofiber meshes on the formation of self-aligned skeletal muscle myotubes. *Biomaterials*. 2008;*29*(19):2899-2906.
29. Beier JP, Klumpp D, Rudisile M, et al. Collagen matrices from sponge to nano: new perspectives for tissue engineering of skeletal muscle. *BMC Biotechnol*. 2009;*9*:34.
30. Kin S, Hagiwara A, Nakase Y, et al. Regeneration of skeletal muscle using in situ tissue engineering on an acellular collagen sponge scaffold in a rabbit model. *ASAIO J*. 2007;*53*(4):506-513.
31. Van Ry PM, Minogue P, Hodges BL, et al. Laminin-111 improves muscle repair in a mouse model of merosin-deficient congenital muscular dystrophy. *Hum Mol Genet*. 2013;*23*(2):383-396.
32. Zou K, De Lisio M, Huntsman HD, et al. Laminin-111 improves skeletal muscle stem cell quantity and function following eccentric exercise. *Stem Cells Transl Med*. 2014;*3*(9):1013-1022.
33. Haas GJ, Dunn AJ, Marcinczyk M, et al. Biomimetic sponges for regeneration of skeletal muscle following trauma. *J Biomed Mater Res A*. 2019;*107*(1):92-103.
34. Dumont FJ. FK506, an immunosuppressant targeting calcineurin function. *Curr Med Chem*. 2000;*7*(7):731-748.
35. Szabo G, Gavala C, Mandrekar P. Tacrolimus and cyclosporine a inhibit allostimulatory capacity and cytokine production of human myeloid dendritic cells. *J Invest Med*. 2001;*49*(5):442-449.
36. Jennings C, Kusler B, Jones PP. Calcineurin inactivation leads to decreased responsiveness to LPS in macrophages and dendritic cells and protects against LPS-induced toxicity in vivo. *Innate Immun*. 2009;*15*(2):109-120.
37. Hurtgen BJ, Henderson BEP, Ward CL, et al. Impairment of early fracture healing by skeletal muscle trauma is restored by FK506. *BMC Musculoskelet Disord*. 2017;*18*(1):253-253.
38. Orth P, Zurakowski D, Alini M, Cucchiarini M, Madry H. Reduction of sample size requirements by bilateral versus unilateral research designs in animal models for cartilage tissue engineering. *Tissue Eng Part C Methods*. 2013;*19*(11):885-891.
39. Goodman CA, Kotecki JA, Jacobs BL, Hornberger TA. Muscle fiber type-dependent differences in the regulation of protein synthesis. *PLoS One*. 2012;*7*(5):e37890.
40. Hurtgen BJ, Ward CL, Garg K, et al. Severe muscle trauma triggers heightened and prolonged local musculoskeletal inflammation and impairs adjacent tibia fracture healing. *J Musculoskelet Neuronal Interact*. 2016;*16*(2):122-134.
41. Fosang AJ, Colbran RJ. Transparency is the key to quality. *J Biol Chem*. 2015;*290*(50):29692-29694.
42. Corona BT, Wu X, Ward CL, McDaniel JS, Rathbone CR, Walters TJ. The promotion of a functional fibrosis in skeletal muscle with volumetric muscle loss injury following the transplantation of muscle-ECM. *Biomaterials*. 2013;*34*(13):3324-3335.
43. Ward CL, Ji L, Corona BT. An autologous muscle tissue expansion approach for the treatment of volumetric muscle loss. *Biores Open Access*. 2015;*4*(1):198-208.
44. Borselli C, Storrie H, Benesch-Lee F, et al. Functional muscle regeneration with combined delivery of angiogenesis and myogenesis factors. *Proc Natl Acad Sci U S A*. 2010;*107*(8):3287-3292.
45. Aurora A, Roe JL, Corona BT, Walters TJ. An acellular biologic scaffold does not regenerate appreciable de novo muscle tissue in rat models of volumetric muscle loss injury. *Biomaterials*. 2015;*67*:393-407.
46. Kasukonis B, Kim J, Brown L, et al. Codelivery of infusion Decellularized skeletal muscle with minced muscle autografts improved recovery from volumetric muscle loss injury in a rat model. *Tissue Eng Part A*. 2016;*22*(19–20):1151-1163.
47. Passipieri JA, Baker HB, Siriwardane M, et al. Keratin hydrogel enhances in vivo skeletal muscle function in a rat model of volumetric muscle loss. *Tissue Eng Part A*. 2017;*23*(11–12):556-571.
48. Sicari BM, Rubin JP, Dearth CL, et al. An acellular biologic scaffold promotes skeletal muscle formation in mice and humans with volumetric muscle loss. *Sci Translational Med*. 2014;*6*(234):234ra58.
49. Corona BT, Machingal MA, Criswell T, et al. Further development of a tissue engineered muscle repair construct in vitro for enhanced functional recovery following implantation in vivo in a murine model of volumetric muscle loss injury. *Tissue Eng Part A*. 2012;*18*(11–12):1213-1228.
50. Corona BT, Ward CL, Baker HB, Walters TJ, Christ GJ. Implantation of in vitro tissue engineered muscle repair constructs and bladder acellular matrices partially restore in vivo skeletal muscle function in a rat model of volumetric muscle loss injury. *Tissue Eng Part A*. 2013;*20*(3–4):705-715.
51. Quarta M, Cromie M, Chacon R, et al. Bioengineered constructs combined with exercise enhance stem cell-mediated treatment of volumetric muscle loss. *Nat Commun*. 2017;*8*:15613.
52. Fishman JM, Lowdell MW, Urbani L, et al. Immunomodulatory effect of a decellularized skeletal muscle scaffold in a discordant xenotransplantation model. *Proc Natl Acad Sci U S A*. 2013;*110*(35):14360-14365.
53. Cheng M, Nguyen MH, Fantuzzi G, Koh TJ. Endogenous interferon-gamma is required for efficient skeletal muscle regeneration. *Am J Physiol Cell Physiol*. 2008;*294*(5):C1183-C1191.
54. Foster W, Li Y, Usas A, Somogyi G, Huard J. Gamma interferon as an antifibrosis agent in skeletal muscle. *J Orthop Res*. 2003;*21*(5):798-804.
55. Londhe P, Davie JK. Gamma interferon modulates myogenesis through the major histocompatibility complex class II transactivator, CIITA. *Mol Cell Biol*. 2011;*31*(14):2854-2866.
56. Deyhle MR, Hyldahl RD. The role of T lymphocytes in skeletal muscle repair from traumatic and contraction-induced injury. *Front Physiol*. 2018;*9*:768.
57. Rayavarapu S, Coley W, Kinder TB, Nagaraju K. Idiopathic inflammatory myopathies: pathogenic mechanisms of muscle weakness. *Skelet Muscle*. 2013;*3*(1):13.
58. Staeheli P, Haller O. Human MX2/MxB: a potent interferon-induced Postentry inhibitor of Herpesviruses and HIV-1. *J Virol*. 2018;*92*(24):e00709-e00718.
59. Skrenta H, Yang Y, Pestka S, Fathman CG. Ligand-independent down-regulation of IFN-gamma receptor 1 following TCR engagement. *J Immunol*. 2000;*164*(7):3506-3511.
60. Spencer MJ, Walsh CM, Dorshkind KA, Rodriguez EM, Tidball JG. Myonuclear apoptosis in dystrophic mdx muscle occurs by perforin-mediated cytotoxicity. *J Clin Invest*. 1997;*99*(11):2745-2751.

61. Venalis P, Lundberg IE. Immune mechanisms in polymyositis and dermatomyositis and potential targets for therapy. *Rheumatology (Oxford)*. 2014;*53*(3):397-405.
62. Kohno S, Ueji T, Abe T, et al. Rantes secreted from macrophages disturbs skeletal muscle regeneration after cardiotoxin injection in Cbl-b-deficient mice. *Muscle Nerve*. 2011;*43*(2):223-229.
63. Zhang J, Xiao Z, Qu C, Cui W, Wang X, du J. CD8 T cells are involved in skeletal muscle regeneration through facilitating MCP-1 secretion and Gr1(high) macrophage infiltration. *J Immunol*. 2014;*193*(10):5149-5160.
64. Hurtgen BJ, Ward CL, Leopold Wager CM, et al. Autologous minced muscle grafts improve endogenous fracture healing and muscle strength after musculoskeletal trauma. *Physiol Rep*. 2017;*5*(14):e13362.
65. Hyldahl RD, Chen TC, Nosaka K. Mechanisms and mediators of the skeletal muscle repeated bout effect. *Exerc Sport Sci Rev*. 2017;*45*(1):24-33.
66. Deyhle MR, Gier AM, Evans KC, et al. Skeletal muscle inflammation following repeated bouts of lengthening contractions in humans. *Front Physiol*. 2015;*6*:424.
67. Murach KA, White SH, Wen Y, et al. Differential requirement for satellite cells during overload-induced muscle hypertrophy in growing versus mature mice. *Skelet Muscle*. 2017;*7*(1):14.
68. Soffe Z, Radley-Crabb HG, McMahon C, Grounds MD, Shavlakadze T. Effects of loaded voluntary wheel exercise on performance and muscle hypertrophy in young and old male C57Bl/6J mice. *Scand J Med Sci Sports*. 2016;*26*(2):172-188.
69. Murach KA, Dungan CM, Peterson CA, McCarthy JJ. Muscle fiber splitting is a physiological response to extreme loading in animals. *Exerc Sport Sci Rev*. 2019;*47*(2):108-115.
70. Lieber RL, Fridén J. Selective damage of fast glycolytic muscle fibres with eccentric contraction of the rabbit tibialis anterior. *Acta Physiol Scand*. 1988;*133*(4):587-588.
71. Webster C, Silberstein L, Hays AP, Blau HM. Fast muscle fibers are preferentially affected in Duchenne muscular dystrophy. *Cell*. 1988;*52*(4):503-513.
72. Kung TA, Cederna PS, Van der Meulen JH, Urbanchek MG, Kuzon WM, Faulkner JA. Motor unit changes seen with skeletal muscle sarcopenia in oldest old rats. *J Gerontol A Biol Sci Med Sci*. 2014;*69*(6):657-665.
73. Corona BT, Flanagan KE, Brininger CM, Goldman SM, Call JA, Greising SM. Impact of volumetric muscle loss injury on persistent motoneuron axotomy. *Muscle Nerve*. 2018;*57*(5):799-807.
74. Chao T, Burmeister DM, Corona BT, et al. Oxidative pathophysiology following volumetric muscle loss injury in a porcine model. *J Appl Physiol (1985)*. 2019;*126*(6):1541-1549.
75. Gehrig SM, Koopman R, Naim T, Tjoakarfa C, Lynch GS. Making fast-twitch dystrophic muscles bigger protects them from contraction injury and attenuates the dystrophic pathology. *Am J Pathol*. 2010;*176*(1):29-33.
76. Orange DE, Blachere NE, Fak J, et al. Dendritic cells loaded with FK506 kill T cells in an antigen-specific manner and prevent autoimmunity in vivo. *Elife*. 2013;*2*:e00105.
77. Pimorady-Esfahani A, Grounds MD, McMenamin PG. Macrophages and dendritic cells in normal and regenerating murine skeletal muscle. *Muscle Nerve*. 1997;*20*(2):158-166.
78. Wirsdörfer F, Bangen JM, Pastille E, et al. Dendritic cell-like cells accumulate in regenerating murine skeletal muscle after injury and boost adaptive immune responses only upon a microbial challenge. *PLoS One*. 2016;*11*(5):e0155870.
79. Corona BT, Rivera JC, Wenke JC, Greising SM. Tacrolimus as an adjunct to autologous minced muscle grafts for the repair of a volumetric muscle loss injury. *J Exp Orthop*. 2017;*4*(1):36.
80. Azizi S, Mohammadi R, Amini K, Fallah R. Effects of topically administered FK506 on sciatic nerve regeneration and reinnervation after vein graft repair of short nerve gaps. *Neurosurg Focus*. 2012;*32*(5):E5.
81. Diaz LM, Steele MH, Guerra AB, et al. The role of topically administered FK506 (tacrolimus) at the time of facial nerve repair using entubulation neurorrhaphy in a rabbit model. *Ann Plast Surg*. 2004;*52*(4):407-413.
82. Venkataramanan R, Jain A, Warty VS, et al. Pharmacokinetics of FK 506 in transplant patients. *Transplant Proc*. 1991;*23*(6):2736-2740.
83. Pollot BE, Goldman SM, Wenke JC, et al. Decellularized extracellular matrix repair of volumetric muscle loss injury impairs adjacent bone healing in a rat model of complex musculoskeletal trauma. *J Trauma Acute Care Surg*. 2016;*81*(5 Suppl 2 Proceedings of the 2015 Military Health System Research Symposium)):S184-S190.
84. Greising SM, Dearth CL, Corona BT. Regenerative and rehabilitative medicine: a necessary synergy for functional recovery from volumetric muscle loss injury. *Cells Tissues Organs*. 2016;*202*(3–4):237-249.

SUPPORTING INFORMATION

Additional supporting information may be found online in the Supporting Information section at the end of this article.

How to cite this article: Haas, G., Dunn, A., Madsen, J., Genovese, P., Chauvin, H., Au, J., Ziemkiewicz, N., Johnson, D., Paoli, A., Lin, A., Pullen, N., & Garg, K. (2021). Biomimetic sponges improve muscle structure and function following volumetric muscle loss. *Journal of Biomedical Materials Research Part A*, 1–14. https://doi.org/10.1002/jbm.a.37212